Dalton Transactions

Accepted Manuscript

Sol-gel syntheses, luminescence, and energy transfer properties of α-GdB_5O_9:Ce^{3+}/Tb^{3+} phosphors

Cite this: DOI: 10.1039/x0xx00000x

Xiaorui Sun,[a] Wenliang Gao,[a] Tao Yang,[a*] and Rihong Cong[a*]

Received 00th January 2012,
Accepted 00th January 2012

DOI: 10.1039/x0xx00000x

www.rsc.org/

Sol-gel method was applied to prepare homogenous and high crystalline phosphors with the formulas α-GdB_5O_9:xTb^{3+} ($0 \leq x \leq 1$), α-$Gd_{1-x}Ce_xB_5O_9$ ($0 \leq x \leq 0.40$), α-GdB_5O_9:xCe^{3+}, $0.30Tb^{3+}$ ($0 \leq x \leq 0.15$) and α-GdB_5O_9:$0.20Ce^{3+}$, xTb^{3+} ($0 \leq x \leq 0.10$). The success syntheses were proved by the linear shrinkage or expansion of the cell volumes against the substitution contents. In α-GdB_5O_9:xTb^{3+}, an efficient energy transfer from Gd^{3+} to Tb^{3+} was observed and there is no luminescence quenching. Besides, the exceptionally high efficiency of the *f-f* excitations of Tb^{3+} implies these phosphors may be good UV-LED phosphors for green-emitting. For α-$Gd_{1-x}Ce_xB_5O_9$, Ce^{3+} absorbs majority of the energy and transfers to Gd^{3+}. Therefore, the co-doping of Ce^{3+} and Tb^{3+} leads to a significant enhancement of the green emission of Tb^{3+}. Our current results together with the study on α-GdB_5O_9:xEu^{3+} in literature indicate that α-GdB_5O_9 is a good phosphor host with advantages including controllable preparation, diverse cationic doping, absence of concentration quenching, and effective energy transfer.

Introduction

Rare earth borates are well known good hosts for luminescent materials due to the high transparency, good thermal stability, exceptional optical damage threshold, and high luminescence efficiency.[1-3] Their major structural characteristic is the rigid covalent B-O network. Polyborates with $B/M \geq 3$ (M = metal) are especially attractive, because the luminescent activators can be well separated in spatial by large polyborates anions and thus the concentration quenching can be postponed.[4,5]

In the Ln_2O_3-B_2O_3 phase diagrams, only three types of borates are obtained by traditional high temperature solid state reaction, including oxyborate,[6] orthoborate[7,8] and metaborate.[9] In contrast, numerous hydrated rare earth polyborates have been prepared by boric acid flux[10,11] or hydrothermal method.[12-18] Those hydrate borates behave as precursors which could transfer to new types of anhydrous borates by thermal decompositions at appropriate conditions.[10,11] For example, α-LnB_5O_9 (Ln = Pr-Eu) was first prepared by a long-time calcination of $H_3LnB_6O_{12}$ at 650-700 ºC for 5 days.[10] Moreover, similar annealing treatments on $Ln[B_8O_{11}(OH)_5]$ (Ln = La-Nd) and $Ln[B_9O_{13}(OH)_3]$•H_2O (Ln = Pr-Eu) led to α-LnB_5O_9 (Ln = Pr-Eu) or β-LnB_5O_9 (Ln = La, Ce), respectively, depending on the size of rare earth cation.[11] In literature, a vacuum-ultraviolet luminescence study on Eu^{3+} doped α-GdB_5O_9 revealed an effective energy transfer from Gd^{3+} to Eu^{3+} in this series of phosphors.[10] However, the major problem is the very long period of the preparation.

Recently, we applied similar thermal decomposition procedures on $Sm_{1-x}Eu_x[B_9O_{13}(OH)_4]$•$H_2O$ and $Gd_{1-x}Eu_x[B_6O_9(OH)_3]$ to prepared α-LnB_5O_9:Eu^{3+} phosphors, where the heating processes were reduced to 10 hours.[19,20] In addition, sol-gel method was also employed to prepare complete α-$Ln_{1-x}Eu_xB_5O_9$ (Ln = Sm and Gd) solid solutions, noting that the traditional solid state reaction method would always lead to a mixture of α-$Ln_{1-x}Eu_xB_5O_9$ and orthoborates/metaborates. In fact, the phosphors prepared by sol-gel method gives a superior luminescence intensity due to its high homogeneity and crystallinity.[19,20]

It becomes apparent that α-LnB_5O_9 is a good host material for luminescence application, because the large polyborate anions prevent the concentration quenching and all the samples investigated by now show strong emission profiles.[10,20] It is interesting to study the performance of another important activator Tb^{3+} in this host. There exists α-TbB_5O_9,[10] which gives an indication of the easy substitution of Tb^{3+} into α-LnB_5O_9. Indeed, we successfully prepared complete solid solutions of α-$Gd_{1-x}Tb_xB_5O_9$ ($0 \leq x \leq 1$) by sol-gel method, whose UV-photoluminescence properties were studied systemically. Moreover, the luminescence efficiency of Tb^{3+} was significantly improved by co-doping of Ce^{3+}. To understand the energy transfer scheme between Gd^{3+}, Ce^{3+} and Tb^{3+}, the luminescent spectra of α-$Gd_{1-x}Ce_xB_5O_9$ ($x \leq 0.40$) and two series of Tb^{3+}, Ce^{3+} co-doped α-GdB_5O_9 were also studied in detail.

Experimental

All phosphors investigated in this study were synthesized by sol-gel method. Stoichiometric Gd_2O_3, Tb_4O_7 (or $Ce(NO_3)_3$•$6H_2O$) were first dissolved by concentrated HNO_3 aqueous solution under stirring and heating. Then, H_3BO_3 (with 10 mol% excess, in order to compensate for the volatilization of boron oxide at high temperature) and an appropriate amount of citric acid and deionized water were added into the solution. After carefully evaporating the water, a clear and homogeneous sol was formed, which was further loaded into an

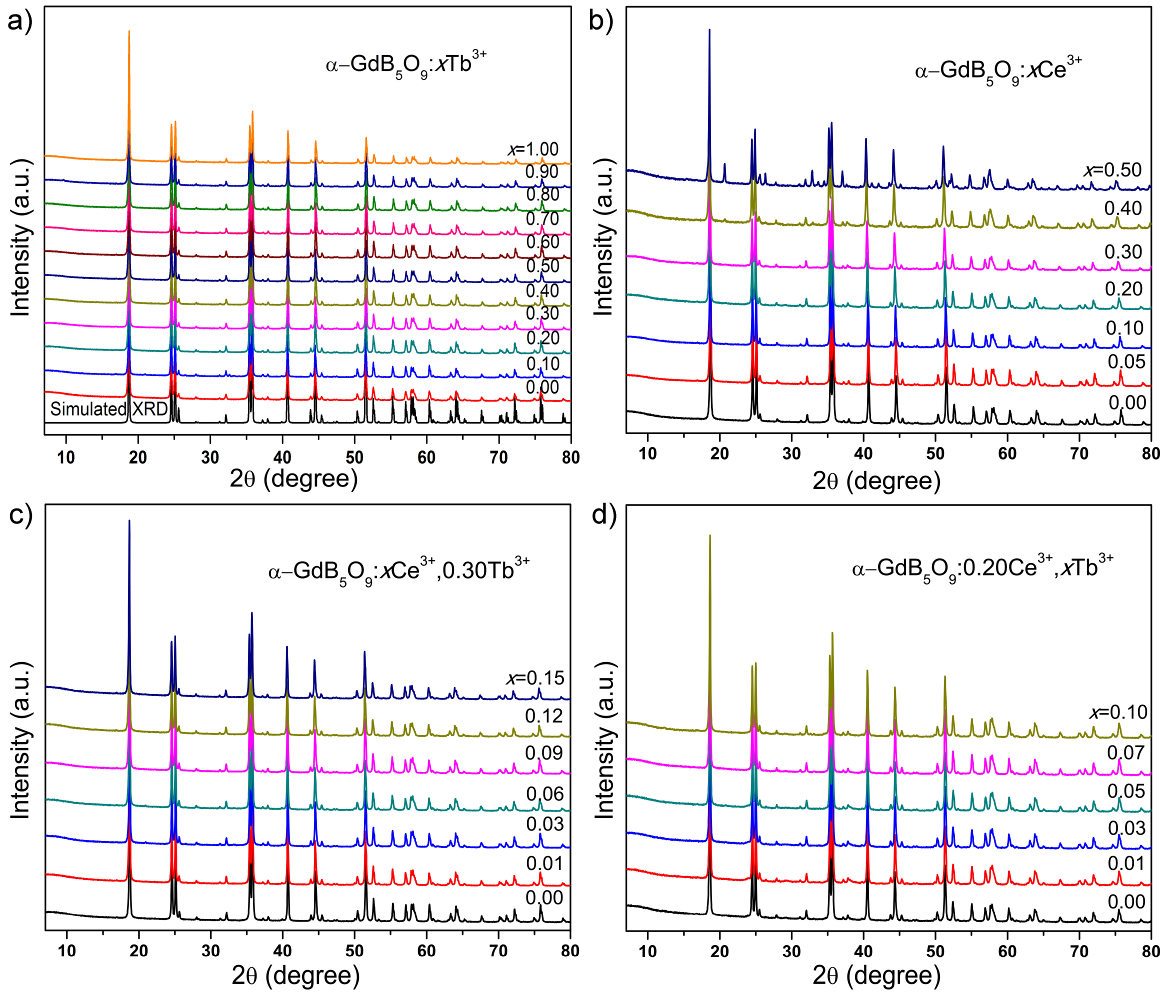

Figure 1 X-ray diffraction patterns of (a) α-GdB_5O_9:$x$$Tb^{3+}$ ($0 \le x \le 1$), (b) α-$Gd_{1-x}Ce_xB_5O_9$ ($0 \le x \le 0.50$), (c) α-GdB_5O_9:$x$$Ce^{3+}$, 0.30$Tb^{3+}$ ($0 \le x \le 0.15$), (d) α-GdB_5O_9:0.20Ce^{3+}, $x$$Tb^{3+}$ ($0 \le x \le 0.10$). It should be noted that a simulated XRD pattern based on the GdB_5O_9 crystal structure is also presented at the bottom of (a).

oven at 80 ºC, 120 ºC and 180 ºC for 5 hours, respectively. A light-brown precursor was obtained. The precursor was then heated in a muffle furnace at 550 ºC for 15 hours, and 670 ºC for 10 hours to obtain the target pentaborate. The final resultant powder was white in color. This synthesis procedure is an inorganic route of the sol-gel process.

Powder XRD data were collected at room temperature on a PANalytical X'pert diffractometer equipped with a PIXcel 1D detector (Co Kα radiation). The operating voltage and current are 40 kV and 40 mA, respectively. Le Bail refinements were performed to obtain the cell parameters using TOPAS software package.[21] Scanning electron microscope images were taken using JSM-7800F electron microscope. Photoluminescent spectra were measured on a Hitachi F4600 fluorescence spectrometer. The voltage of Xe lamp is fixed to be 700 V. The emission intensities are calculated from the integral of corresponding peaks. The internal quantum efficiency (QE) was measured in the same instrument with a spectrum calibration. White $BaSO_4$ powder was used as a reference to measure the absorption. It can be calculated by the following equation.[22,23]

$$Q = \int L_S / \int E_R - \int E_S$$

Where $\int L_S$ is the integrated intensity of the photoluminescence spectrum for the sample; $\int E_R$ and $\int E_S$ are the integrated intensity of the reflectance spectra for $BaSO_4$ powder and the sample, respectively.

Results and discussion

Phase identification and purity

Figure 1 shows the powder XRD patterns of α-GdB_5O_9 with substantial doping of Tb^{3+} and/or Ce^{3+}, and the sharp peaks point to the high crystallinity of as-prepared samples. For α-$Gd_{1-x}Tb_xB_5O_9$ ($0 \le x \le 1$), it is evident that pure phase of α-LnB_5O_9 was formed without any impurity peak, by comparing to the simulated XRD pattern for GdB_5O_9 (see Figure 1a). Because of the similar cationic radii for Gd^{3+} and Tb^{3+}, it is expected to form complete solid solutions. The peak shift by Tb^{3+}-doping is not that obvious, we could determine the change of the cell lattice parameters (a, c and V) by careful refinements on the whole powder XRD patterns (See Table S1 in the supporting information). The plot of the cell volume along with the increase of x (see Figure 2a) suggests a linear shrinkage. These results evidently confirm that Tb^{3+} has been successfully incorporated into α-GdB_5O_9 without any structural change.

In literature, the sol-gel method always leads to a high crystallinity of the resultant sample. Here, SEM images were taken on a representative sample with the formula α-$Gd_{0.7}Tb_{0.3}B_5O_9$ (See Figure 3). Intrinsically, the powder sample contains large particles in micrometers, which are in fact aggregators of small nanocrystals. The dimensions of these nanocrystals are close to each other, which is 100~200 nm in width and 300~500 nm in length. An elemental analysis was performed on this sample which gave an average atomic ratio of Gd : Tb = 0.70 : 0.30 (see the insert of Figure 3a).

As shown in Figure 1b, only partial solid solutions of α-$Gd_{1-x}Ce_xB_5O_9$ ($0 \leq x \leq 0.40$) can be obtained. For example, the patterns with x = 0.05-0.30 are almost identical with that of α-GdB_5O_9, however some small impurity peaks emerge when x = 0.40, and their intensities increase significantly when x = 0.50. These impurity peaks were identified to α-CeB_3O_6. Then, it indicates that the doping

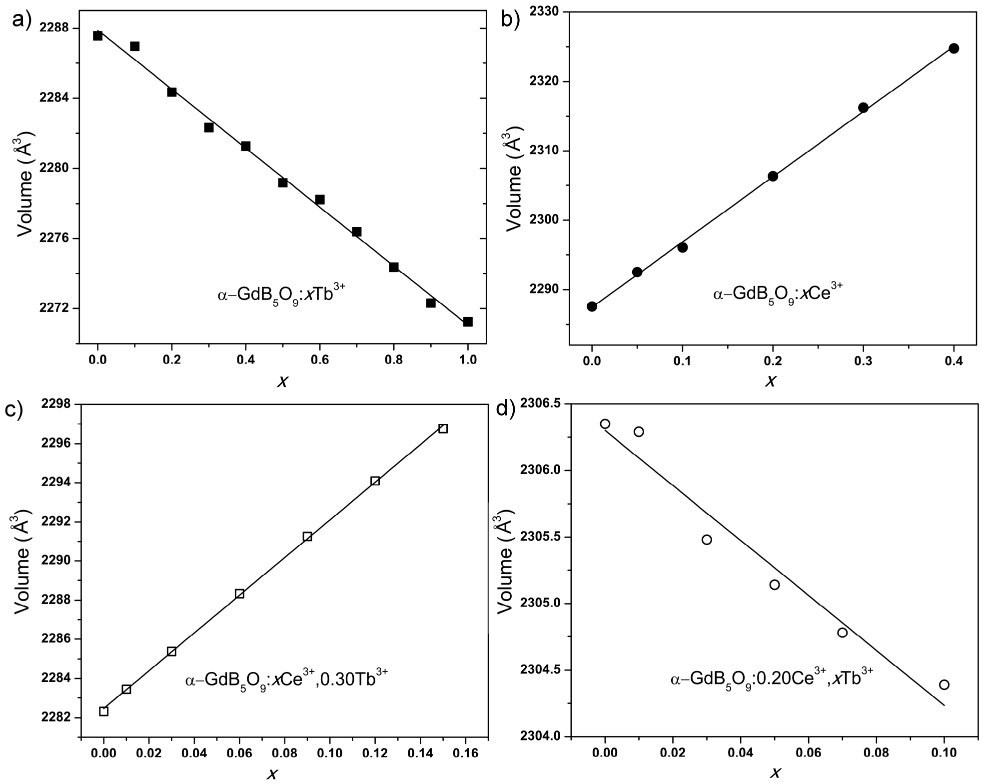

Figure 2 The unit cell volumes refined from the Le Bail fitting change along with the doping content (x), including (a) α-GdB_5O_9:xTb^{3+} ($0 \leq x \leq 1$), (b) α-$Gd_{1-x}Ce_xB_5O_9$ ($0 \leq x \leq 0.50$), (c) α-GdB_5O_9:xCe^{3+}, $0.30Tb^{3+}$ ($0 \leq x \leq 0.15$), (d) α-GdB_5O_9:$0.20Ce^{3+}$, xTb^{3+} ($0 \leq x \leq 0.10$).

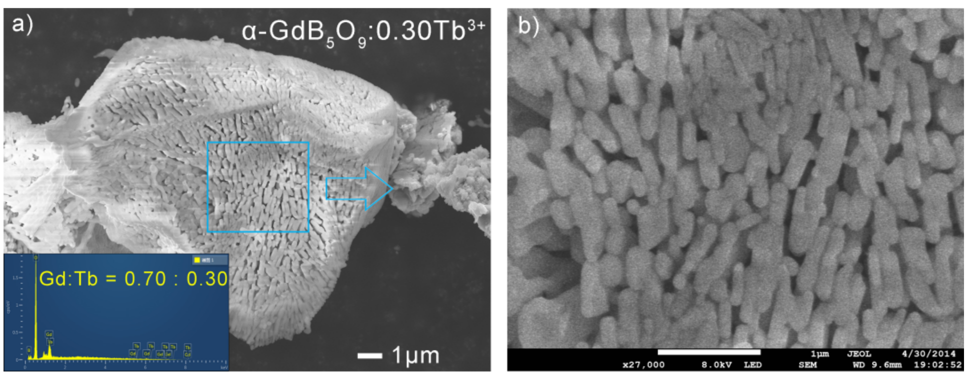

Figure 3 SEM images for α-GdB_5O_9:$0.30Tb^{3+}$ sample, where the EDX spectrum is shown as an insert.

upper limit for Ce^{3+} in α-GdB_5O_9 is around 40 atom%. As reported in literature,[11] CeB_5O_9 crystallizes in another structure type, named β-polymorph (monoclinic, $P2_1/c$), which should be the reason for not getting whole solid solutions of α-$Gd_{1-x}Ce_xB_5O_9$. Le Bail refinements on powder XRD patterns for α-$Gd_{1-x}Ce_xB_5O_9$ were performed to obtain the cell lattice parameters (see Table S2 and Figure 2b). There is a clear expanding tendency with the increasing substitution from $x = 0$ to $x = 0.40$, which is consistent with the increase of the ionic radii from Gd^{3+} to Ce^{3+}.

Two series of Ce^{3+} and Tb^{3+} co-doped α-GdB_5O_9 samples were also prepared in order to understand the energy transfer pathways. One is fixing the concentration of Tb^{3+} at 0.30 and making the content of Ce^{3+} flexible from 0 to 0.15, and the other is fixing the concentration of Ce^{3+} at 0.20 while changing the Tb^{3+} content from 0 to 0.10. Figures 1c and 1d give the powder XRD patterns of these as-synthesized products, respectively. All samples are pure as no obvious impurity peaks can be found. The refined unit cell parameters are listed in Table S3 and S4. The cell volumes against the substitution levels were shown in Figures 2c and 2d. The linear evolution behaviors on parameters confirm the successful cationic substitution. In summary, the easy substitution of Tb^{3+} and Ce^{3+} into α-GdB_5O_9 prove that sol-gel method is an efficient way to prepare α-GdB_5O_9 type phosphors, due to its relatively short reaction time, controllable doping content, high homogeneity and crystallinity.

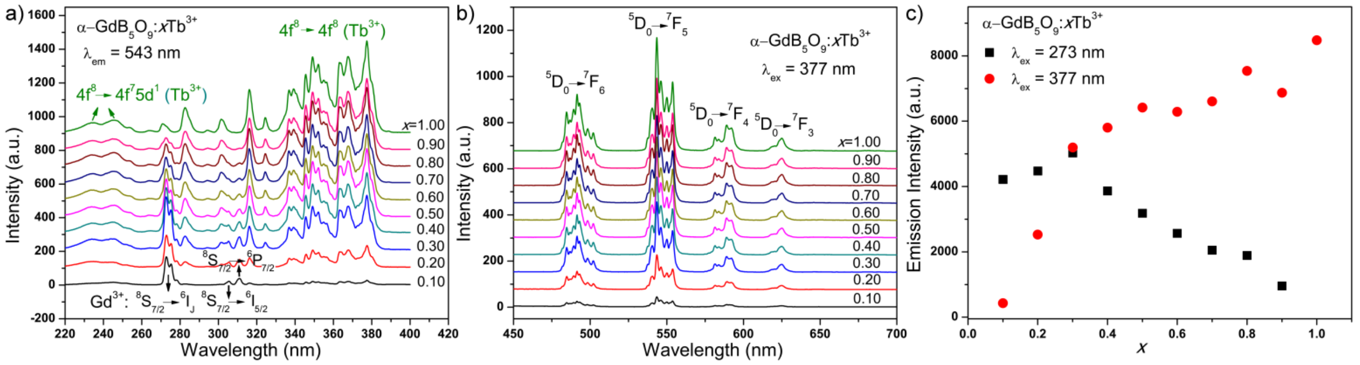

Figure 4 (a) Excitation and (b) emission spectra of the α-GdB_5O_9:xTb^{3+} ($0 \le x \le 1$) samples. (c) Dependence of the emission intensity excited at 273 and 377 nm against the doping concentration x.

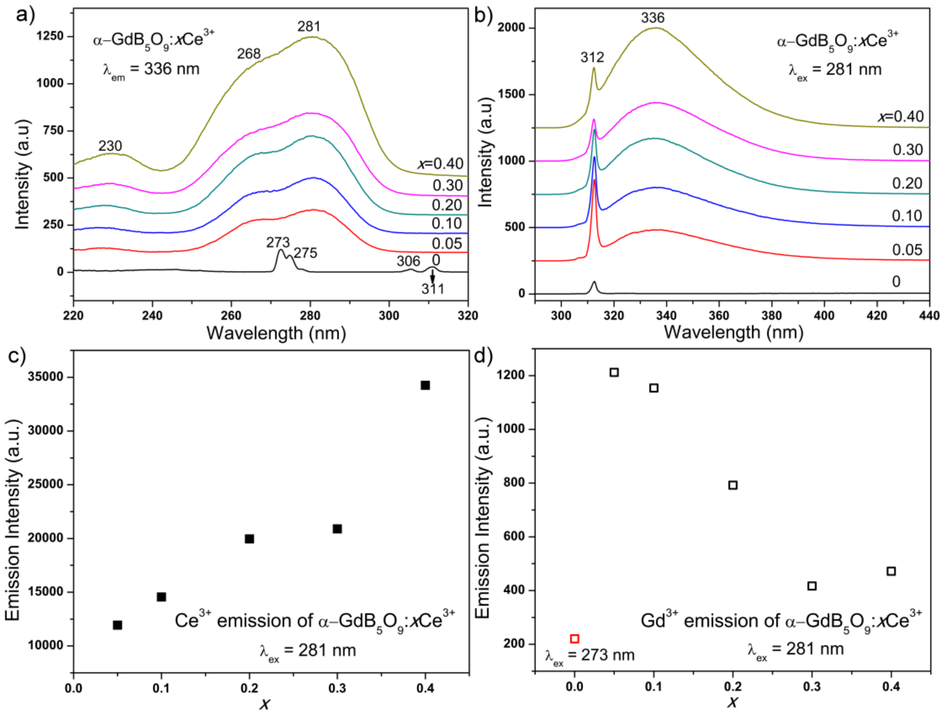

Figure 5 (a) Excitation and (b) emission spectra of the α-GdB_5O_9:xCe^{3+} ($0 \le x \le 0.40$) samples. Dependence of the emission intensities for (c) Ce^{3+} emission and (d) Gd^{3+} emission against the doping concentration x. Note that the emission spectrum was collected under the 273 nm excitation when $x = 0$.

Luminescent properties and energy transfer in α-GaB$_5$O$_9$:xTb^{3+} (x = 0.10-1.00)

Figure 4a presents the excitation spectra of α-GdB$_5$O$_9$:xTb^{3+} (x = 0.10-1.00), which were obtained by monitoring the strongest emission at 543 nm. Obviously, the spectrum profile changes gradually with the increase of Tb^{3+} concentration. When x = 1.00, all of the peaks can be readily attributed to the absorption of Tb^{3+}. The broad bands in the range of 220-260 nm can be assigned to the typical $4f^8 \rightarrow 4f^7 5d^1$ transitions of Tb^{3+}, and those sharp peaks in the higher wavelength region of 260-390 nm are owing to the $4f^8 \rightarrow 4f^8$ transitions of Tb^{3+}, respectively.[24] In literature, most Tb^{3+}-phosphors usually have much stronger *f-d* band absorptions than the *f-f* transitions, because the former transitions are usually spin-allowed while the latter ones are forbidden.[25,26] However, it is opposite in α-GdB$_5$O$_9$:xTb^{3+}, where the *f-f* absorptions are very strong, indicating these transitions are parity-allowed. We speculate that this might be attributed to the noncentrosymmetric local environment of Tb^{3+} in α-*Ln*B$_5$O$_9$.[10] It is important because this characteristic of α-GdB$_5$O$_9$:xTb^{3+} is in fact favored to be excited by near-UV LED chips (350-420 nm) and produce appropriate green-emitting phosphors for WLEDs.

For those samples with low Tb^{3+} concentrations, i.e. x = 0.10, some sharp peaks (273, 275, 306 and 311 nm) belong to Gd^{3+} absorption can be readily observed,[27] which indicates an energy transfers from Gd^{3+} to Tb^{3+} in this series of compounds. With the increase of Tb^{3+} concentration, the intensities of Gd^{3+} absorptions increase first, which reaches a maximum when x = 0.30 and then become weaker.

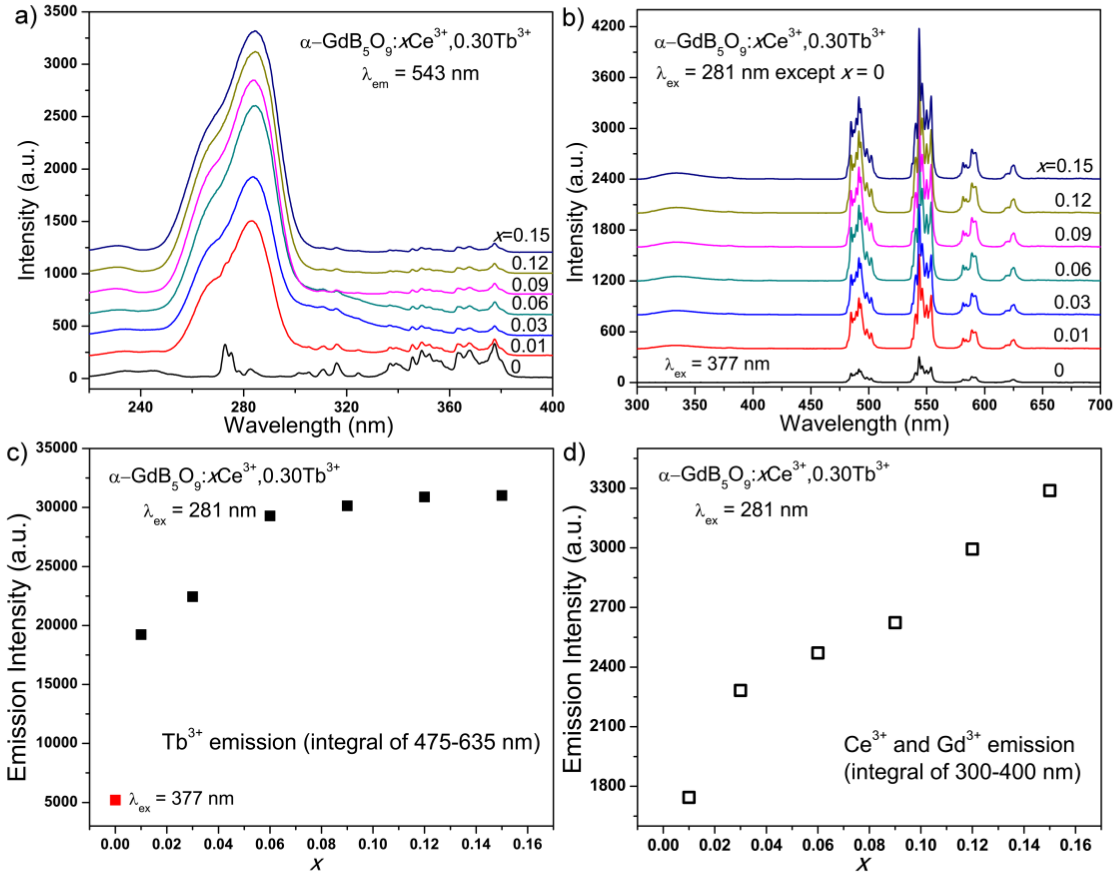

Figure 6 (a) Excitation and (b) emission spectra of the α-GdB$_5$O$_9$:xCe^{3+}, 0.30Tb^{3+} ($0 \leq x \leq 0.15$) samples. Dependence of the emission intensity of (c) Tb^{3+} emission and (d) Ce^{3+}/Gd^{3+} emission against the doping concentration x. Note that the emission spectrum was collected under the 377 nm excitation when x = 0.

As shown in Figure 4b, the emission spectra of α-GdB$_5$O$_9$:xTb^{3+} (x = 0.10-1.00) show a similar characteristic under the excitation of 377 nm (*f-f* transition of Tb^{3+}). Typically, four groups of emission peaks at about 478-512, 528-562, 576-602, and 614-635 nm were readily attributed to the typical $^5D_4 \rightarrow {}^7F_J$ (J = 6-3) transitions of Tb^{3+} ion, respectively.[22] The dominated one appears at 543 nm, so these phosphors show bright green emissions. The influences of Tb^{3+} concentration on the total emission intensity of the phosphors are shown in Figure 4c. It is obvious that no concentration quenching or saturation effect is observed, when excited by 377 nm (*f-f* transition of Tb^{3+}). Similar phenomena have been observed in α-$Sm_{1-x}Eu_xB_5O_9$ and α-$Gd_{1-x}Eu_xB_5O_9$ (λ_{ex} = 392 nm).[19,20] This is reasonable because the Tb^{3+} ions are well separated by pentaborate groups.[10] If excited by 273 nm irradiation (Gd^{3+} absorption), the emission intensity increases with Tb^{3+} content first and reaches a maximum value when x = 0.30 (see Figures 4c and S1 in the supporting information). We think this evolution tendency is related with the efficiency of energy transfer from Gd^{3+} to Tb^{3+}, which reaches the optimal value when x = 0.30.

Luminescent properties and energy transfer in α-GdB_5O_9:$x$$Ce^{3+}$ (x = 0.05-0.40)

The excitation and emission spectra of α-GdB_5O_9:$x$$Ce^{3+}$ (x = 0-0.40) are shown in Figures 5a and 5b, respectively. The excitation pectra of Ce^{3+} doped α-GdB_5O_9 (x = 0.05-0.40) by monitoring 336 nm emission contains three broad bands from 220 nm to 310 nm, which are derived from the 4f-5d transitions of Ce^{3+}.[24] The absorption intensity increases gradually with the increase of Ce^{3+} doping concentration. By comparing these excitation spectra with that of host α-GdB_5O_9, it can be found that no additional Gd^{3+} absorption was observed in these Ce^{3+} doped samples, which is different with the case in α-GdB_5O_9:$x$$Tb^{3+}$. The absence of Gd^{3+} absorption by monitoring Ce^{3+} emission indicates there is no energy transfer from Gd^{3+} to Ce^{3+}.

In emission spectra, a broad and asymmetric violet band emission with a maximum at about 336 nm was observed under the excitation of 281 nm, which is characteristic $4f^05d^1$-$4f^1$ ($^2F_{5/2}$ and $^2F_{7/2}$) transitions of Ce^{3+}.[24] Therefore, the Stokes shift could be roughly estimated to be ~55 nm by assuming that the excitation band is the mirror image of the emission band. Besides, a sharp peak at 312 nm was found in the left shoulder of the emission band. This peak was also observed in the emission spectrum of α-GdB_5O_9, therefore it is attributed to the ^6P_J-$^8S_{7/2}$ transition of Gd^{3+}. Obviously, the appearance of Gd^{3+} emission under the excitation of Ce^{3+} absorption suggests an energy transfer from Ce^{3+} to Gd^{3+}, which is rare.

In order to further understand the competitive behavior between Gd^{3+} and Ce^{3+} in α-GdB_5O_9:$x$$Ce^{3+}$, the dependence of the emission intensities of Ce^{3+} and Gd^{3+} on x have been plotted in Figures 5c and 5d. The emission intensity of Gd^{3+} was calculated from the integral of the corresponding peak at 312 nm with a deduction of Ce^{3+} emission band. And, the emission intensity of Ce^{3+} was then calculated by the total integration of 300-400 nm after subtracting the Gd^{3+} emission. First, the emission intensity of Ce^{3+} increases monotonously along with the increase of x. No quenching or saturation effects was observed, which is similar with the situation of Tb^{3+}-doping. Second, Ce^{3+} ions were incorporated to replace Gd^{3+}, therefore the content of Gd^{3+} was reduced when x increases. Usually, the intensity of Gd^{3+} emission should decrease when x increases. It is the case that a decline occurs in the range of x = 0.05-0.30. However, the emission intensity of Gd^{3+} for pure α-GdB_5O_9 is very weak, which is enhanced about five times after Ce^{3+}-doping (x = 0.05). This is an indication of the existence of an energy transfer from Ce^{3+} to Gd^{3+}.

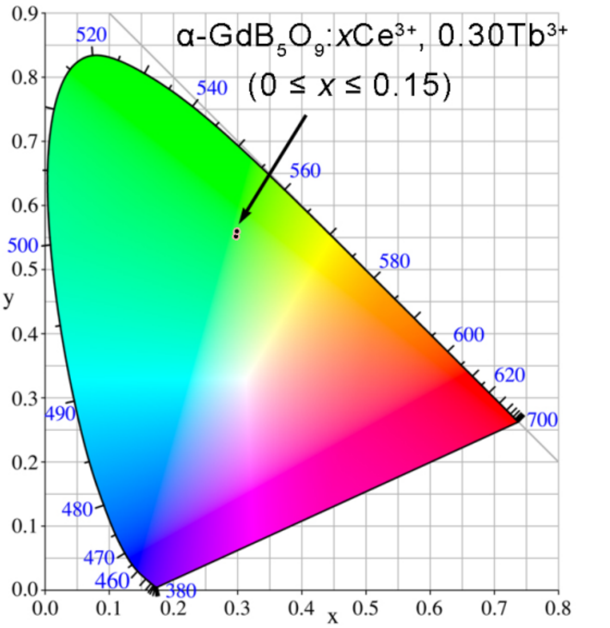

Figure 7 CIE chromaticity coordinates of α-GdB_5O_9:$x$$Ce^{3+}$, 0.30$Tb^{3+}$ ($0 \le x \le 0.15$) samples excited by 281 nm irradiation. When x = 0, the excitation wavelength is 377 nm.

In summary, both Gd^{3+} and Tb^{3+} can be excited by the incident photons in α-GdB_5O_9:$x$$Tb^{3+}$, and the energy absorbed by Gd^{3+} can be efficiently transferred to Tb^{3+} activators; when Ce^{3+} was doped into α-GdB_5O_9, only Ce^{3+} absorption can be observed, and the energy was partially transferred to Gd^{3+}, which results in the co-existence of Ce^{3+} and Gd^{3+} emissions in the spectra.

Energy transfer in Ce^{3+}, Tb^{3+} co-doped α-GdB_5O_9

As shown above, Ce^{3+} doped samples exhibit strong blue emission in the range of 300-400 nm; Tb^{3+} doped samples have intense absorptions ranging from 270 to 380 nm. Obviously, there is an overlap in spectra between the emission of Ce^{3+} and the excitation of Tb^{3+}, which suggests an effective resonance-type energy transfer from Ce^{3+} to Tb^{3+} in α-GdB_5O_9 phosphors.[24,26]

Figures 6a and 6b show the emission spectra of samples with fixed Tb^{3+} concentration at 30% and variable Ce^{3+} concentrations, α-GdB_5O_9:$x$$Ce^{3+}$, 0.30$Tb^{3+}$ (x = 0, 0.01, 0.03, 0.06, 0.09, 0.12, and 0.15). Most spectra show similar characteristic profiles with different Ce^{3+} doping contents except x = 0. For example, the excitation spectrum of α-GdB_5O_9:0.01Ce^{3+}, 0.30Tb^{3+} (by monitoring the emission of Tb^{3+} at 543 nm) show all absorptions from Ce^{3+}, Gd^{3+} and Tb^{3+}. First, the presence of intense Ce^{3+} absorption band supports the existence of very effective energy transfer from Ce^{3+} to Tb^{3+}. Second, Gd^{3+} can also absorb photon energy and transfer to Tb^{3+}. The emission spectrum of α-GdB_5O_9:0.01Ce^{3+}, 0.30Tb^{3+} under the 281 nm irradiation (Ce^{3+} absorption) exhibits strong green emission peaks (4f-4f transitions of Tb^{3+} ions), weak blue emission band (5d-4f transitions of Ce^{3+}), and ^6P_J-$^8S_{7/2}$ transition of Gd^{3+}. The small and residual Ce^{3+} emission indicates the energy transfer from Ce^{3+} to Tb^{3+} is very efficient but may not be complete.

For clarity, the emission intensities of Tb^{3+} and Ce^{3+} (including Gd^{3+}) transitions were calculated, and Figures 6c and 6d show their dependence on the Ce^{3+} content (x). Although the concentration of Tb^{3+} is fixed, the emission intensity of Tb^{3+} remarkably increases with increasing Ce^{3+} concentration, and reaches its maximum when x = 0.06, which then maintains almost constant in the range of x = 0.06-0.15. As expected, the intensity of the green emission in Tb^{3+}, Ce^{3+} co-doped phosphors, i.e. α-GdB_5O_9:0.06Ce^{3+}, 0.30Tb^{3+}, is greatly enhanced in comparison with that of Tb^{3+} solely doped phosphor, which confirms a high efficient energy transfer from Ce^{3+} to Tb^{3+}. The emission saturation behavior when $x > 0.06$ is probably due to limited Tb^{3+} concentration in this case. Moreover, a monotonous increase of Ce^{3+} and Gd^{3+} emission intensity along with the increase of x was also observed, as shown in Figure 6d. It can be seen that the emission intensities of Ce^{3+} and Gd^{3+} are only 10% of that of Tb^{3+}. So, these phosphors do not show an obvious color change, as shown in the chromaticity diagram (see Figure 7). For clarity, the exact coordination values are present in Table S5.

Figures 8a and 8b show the excitation and emission spectra of α-GdB_5O_9:0.20Ce^{3+}, $x$$Tb^{3+}$ (x = 0, 0.01, 0.03, 0.05, 0.07, and 0.10, respectively). The excitation spectra profiles are similar to that of Ce^{3+} solely doped sample, except that the relative absorption intensities are different. Under the excitation of 281 nm, the ratio between blue emission of Ce^{3+} and green emission of Tb^{3+} changes when x increases from 0 to 0.10. Figures 8c and 8d give the influence of x on the emission intensities of Tb^{3+} and Ce^{3+} (including Gd^{3+}). With increasing Tb^{3+} concentration (x), the emission intensity of Tb^{3+} increases sharply first and slows down thereafter. On the contrast, the emission intensity of Ce^{3+} (and Gd^{3+}) firstly decreases substantially with x changes from 0 to 0.01, which then declines slowly with increasing x. The CIE chromaticity coordinates for the phosphors are also calculated from the emission spectra and presented in Figure 9 and Table S5. One can see the luminescence color was changed from blue to green suddenly by only introducing 1 atom% Tb^{3+} ions, while the CIE chromaticity coordinates of α-GdB_5O_9:0.20Ce^{3+}, $x$$Tb^{3+}$ (x = 0.01, 0.03, 0.05, 0.07, and 0.10) are very close to each other. This phenomenon indicates that most of the energy absorbed by Ce^{3+} is transformed to Tb^{3+} and thus Tb^{3+} gives a very strong green luminescence.

Internal quantum efficiency

Table 1 summarizes the internal QE values for various phosphors. The QE values of α-GdB_5O_9:$x$$Tb^{3+}$ phosphors were measured under 377 nm excitation and the emission is in the range of 450-700 nm. High QE values were observed (88% and 75% when x = 0.30 and 1.00, respectively), indicating that α-GdB_5O_9:$x$$Tb^{3+}$ are promising candidates for UV-LED phosphors.

The excitation and emission for Ce^{3+} and Tb^{3+} co-doped samples were set to be 281 nm and in the range of 290-700 nm, respectively. It is found that the QE values of α-GdB_5O_9:$x$$Ce^{3+}$, 0.30$Tb^{3+}$ decrease with the increase of Ce^{3+} content. Besides, a low QE value of 17% was obtained for α-GdB_5O_9:0.20Ce^{3+}, showing the energy absorbed by Ce^{3+} was mostly lost by non-radiative transitions. By co-doping Tb^{3+} in α-GdB_5O_9:0.20Ce^{3+}, $x$$Tb^{3+}$ phosphors, the QE values increase from x = 0 to x = 0.03, and then almost keep as a constant. The QE values of two bright phosphors (α-GdB_5O_9:0.15Ce^{3+}, 0.30Tb^{3+} and α-GdB_5O_9:0.20Ce^{3+}, 0.10Tb^{3+}) are 54% and 48%, respectively. Moreover, the emission intensity of α-GdB_5O_9:0.15Ce^{3+}, 0.30Tb^{3+} is 5.96 times as large as that of α-GdB_5O_9:0.30Tb^{3+}, and the emission intensity of α-GdB_5O_9:0.20Ce^{3+}, 0.10Tb^{3+} is 7.41 times as large as that of α-GdB_5O_9:0.10Tb^{3+}. All these results demonstrate that efficient energy transfer occurs between Ce^{3+} and Tb^{3+}, which is benefit for enhancing the green emission of Tb^{3+} in phosphors.

Table 1. Internal quantum efficiencies for various α-GdB_5O_9:Ce^{3+}, Tb^{3+} samples.

Sample	Excitation wavelength (nm)	Relative Luminescence intensity	Quantum efficiency (%)
α-GdB_5O_9:100Tb^{3+}	377	1.63	75
α-GdB_5O_9:30Tb^{3+}	377	1.00*	88
α-GdB_5O_9:0.01Ce^{3+}, 0.30Tb^{3+}	281	3.70	61
α-GdB_5O_9:0.12Ce^{3+}, 0.30Tb^{3+}	281	5.94	56
α-GdB_5O_9:0.15Ce^{3+}, 0.30Tb^{3+}	281	5.96	54
α-GdB_5O_9:0.20Ce^{3+}	281	—	17
α-GdB_5O_9:0.20Ce^{3+}, 0.01Tb^{3+}	281	3.97	32
α-GdB_5O_9:0.20Ce^{3+}, 0.03Tb^{3+}	281	6.27	44
α-GdB_5O_9:0.20Ce^{3+}, 0.07Tb^{3+}	281	7.27	49
α-GdB_5O_9:0.20Ce^{3+}, 0.10Tb^{3+}	281	7.41	48

*the emission intensity of α-GdB_5O_9:30Tb^{3+} was normalized to be 1.00.

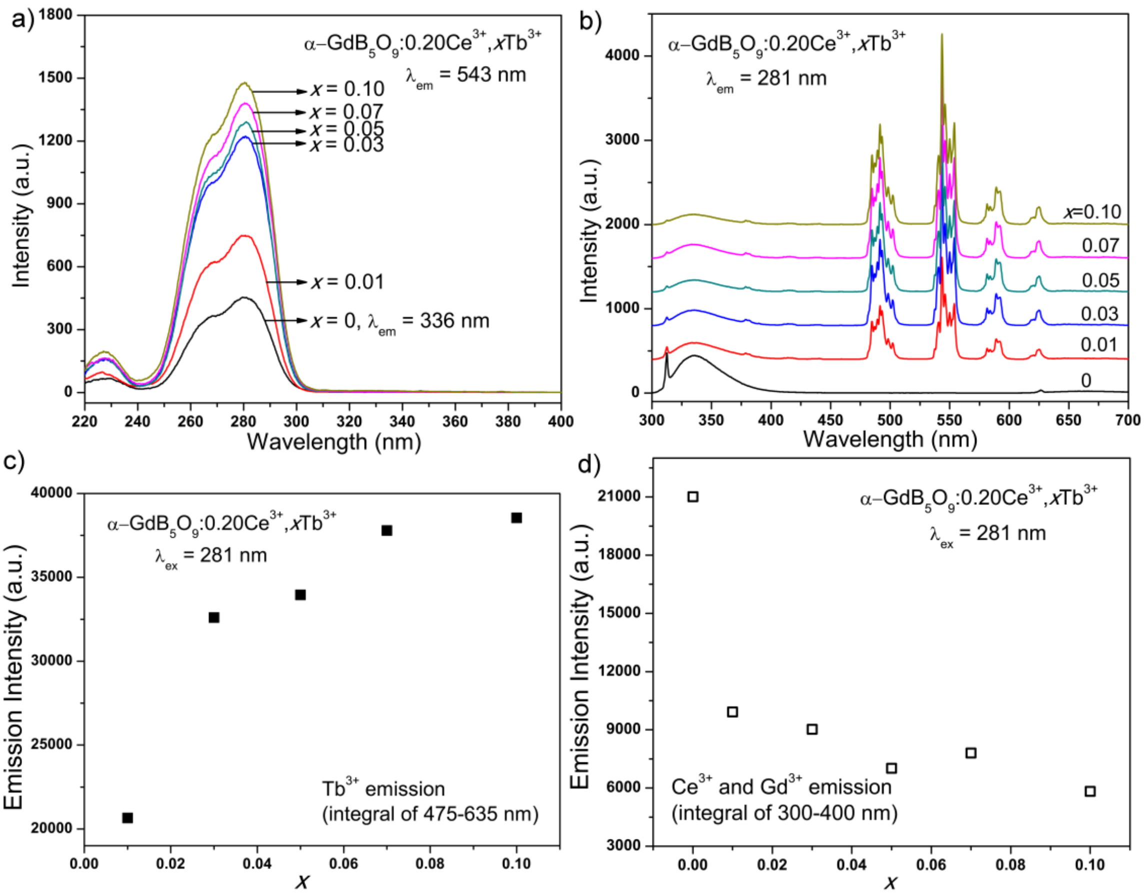

Figure 8 (a) Excitation and (b) emission spectra of the α-GdB_5O_9: $0.20Ce^{3+}$, xTb^{3+} ($0 \leq x \leq 0.10$) samples. Dependence of the emission intensity of (c) Tb^{3+} emission and (d) Ce^{3+} /Gd^{3+} emission against the doping concentration *x*.

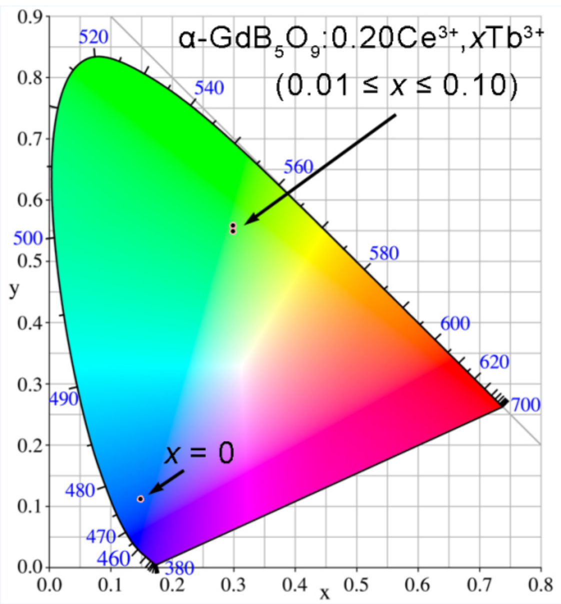

Figure 9 CIE chromaticity coordinates of α-GdB_5O_9:$0.20Ce^{3+}$, xTb^{3+} ($0 \leq x \leq 0.10$) samples excited by the 281 nm irradiation.

Conclusions

In conclusion, four series of solid solutions of α-GdB_5O_9:xTb^{3+} ($0 \leq x \leq 1$), α-$Gd_{1-x}Ce_xB_5O_9$ ($0 \leq x \leq 0.40$), α-GdB_5O_9:xCe^{3+}, $0.30Tb^{3+}$ ($0 \leq x \leq 0.15$), α-GdB_5O_9:$0.20Ce^{3+}$, xTb^{3+} ($0 \leq x \leq 0.10$) were synthesized by employing the sol-gel method. The linear shrinkage or expansion of the cell volumes against the substitution contents proves that the cationic doping to α-GdB_5O_9 is controllable with high homogeneity and crystallinity. The expected efficient energy transfer from Gd^{3+} to Tb^{3+} and the absence of luminescence quenching were confirmed for α-GdB_5O_9:xTb^{3+}. Besides, the exceptionally high efficiency of the *f-f* excitations of Tb^{3+} implies these phosphors may be good UV-LED phosphors for green-emitting. Furthermore, intense UV absorptions and blue emission can be acquired in α-$Gd_{1-x}Ce_xB_5O_9$ phosphors. Interestingly, a possible energy transfer from Ce^{3+} to Gd^{3+} was suggested by the coexistence of Gd^{3+} and Ce^{3+} emission. In Ce^{3+} and Tb^{3+} co-doped α-GdB_5O_9 phosphors, the green emission of Tb^{3+} is significantly improved with the incorporation of Ce^{3+} sensitizers. Ce^{3+} can strongly absorb UV irradiation and transfer its energy to Tb^{3+} in a high efficient way, resulting in the increase of Tb^{3+} green emission and also a weak Ce^{3+} emission in the blue region. Therefore, the corresponding CIE coordinates of co-doped phosphors is in the green regions and keep almost constant. Overall, our current results together with the study on α-GdB_5O_9:$x$$Eu^{3+}$ in literature indicate that α-GdB_5O_9 is a good phosphor host with advantages of controllable preparation, diverse cationic doping, absence of concentration quenching, and effective energy transfer.

Acknowledgements

This work was financially supported by the Nature Science Foundation of China (Grants 91222106, 21101175, 21171178) and Natural Science Foundation Project of Chongqing (Grants 2012jjA0438, 2014jcyjA50036). The Fundamental Research Funds for the Central Universities (Grant CQDXWL-2014-005) also partially supported this work.

Notes and references

[a] College of Chemistry and Chemical Engineering, Chongqing University, Chongqing 400044, People's Republic of China. Corresponding author, Email: congrihong@cqu.edu.cn, taoyang@cqu.edu.cn; Tel: +86-23-65105065.

Electronic Supplementary Information (ESI) available: Tables of cell parameters obtained by Le Bail refinements for all solid solutions, CIE chromaticity coordinates for phosphors, Emission spectra of the α-GdB_5O_9:$x$$Tb^{3+}$ ($0 \le x \le 1$) samples under 273 nm excitation. See DOI: 10.1039/b000000x/

1. B. Saubat, C. Fouassier, P. Hagenmuller and J. C. Bourcet, *Mater. Res. Bull.*, 1981, **16**, 193–198.
2. K. Machida, G. Adachi and J. Shiokawa, *J. Lumin*., 1979, **21**, 101–110.
3. W. Z. Pei, Q. Su and J. Y. Zhang, *J. Alloys Compd*., 1993, **198**, 51–53.
4. Z. Yang, J. H. Lin and M. Z. Su, *Acta Chemica Sinica*, 2001, **59**, 736-741.
5. M. He, G. L. Huang, H. L. Tao and Z. H. Zhang, *Physica B*, 2012, **407**, 2725-2728.
6. E. M. Levin, C. R. Robbins and J. L. Waring, *J. Am. Ceram. Soc.*, 1961, **44**, 87-91.
7. J. H. Lin, M. Z. Su, K. Wurst and E. Schweda, *J. Solid State Chem.*, 1996, **126**, 287-291.
8. J. H. Lin, S. Zhou, L. Q. Yang, G. Q. Yao, M. Z. Su and L. P. You, *J. Solid State Chem.*, 1997, **134**, 158-163.
9. M. Ren, J. H. Lin, Y. Dong, L. Q. Yang, M. Z. Su and L. P. You, *Chem. Mater.*, 1999, **11**, 1576-1580.
10. L. Y. Li, P. C. Lu, Y. Y. Wang, X. L. Jin, G. B. Li, Y. X. Wang, L. P. You and J. H. Lin, *Chem. Mater.*, 2002, **14**, 4963-4968.
11. L. Y. Li, X. L. Jin, G. B. Li, Y. X. Wang, F. H. Liao, G. Q. Yao and J. H. Lin, *Chem. Mater.*, 2003, **15**, 2253-2260.
12. G. K. Abdyllayev, G. G. Dzhafarov and K. S. Mamedov, *Kristallografiya*, 1984, **29**, 1084-1088.
13. E. L. Belokoneva, S. Y. Stefanovich, O. V. Dimitrova and A. G. Ivanova, *Russ. J. Inorg. Chem.*, 2002, **47**, 317-323.
14. A. G. Ivanova, E. L. Beloknoeva and O. V. Dimitrova, *Russ. J. Inorg. Chem.*, 2004, **49**, 816-822.
15. E. L. Beloknoeva, A. G. Ivanova and O. V. Dimitrova, *Russ. J. Inorg. Chem.*, 2006, **51**, 869-877.
16. A. G. Ivanova, E. L. Belokoneva, O. V. Dimitrova and N. N. Mochenova, *Russ. J. Inorg. Chem.*, 2006, **51**, 584-588.
17. A. G. Ivanova, E. L. Belokoneva, O. V. Dimitrova and N. N. Mochenova, *Russ. J. Inorg. Chem.*, 2006, **51**, 862-868.
18. R. H. Cong, T. Yang, Z. M. Wang, J. L. Sun, F. H. Liao, Y. X. Wang and J. H. Lin, *Inorg. Chem.*, 2011, **50**, 1767-1774.
19. X. F. Yi, R. H. Cong, M. F. Yue, Y. Q. Chai, P. F. Jiang, W. L. Gao and T. Yang, *Dalton Trans.*, 2013, **42**, 16318-16327.
20. X. F. Yi, R. H. Cong, Z. Y. Zhou, P. F. Jiang, W. L. Gao and T. Yang, *New J. Chem.*, 2014, **38**, 122-131.
21. *TOPAS*, *V4.1-beta*, Bruker AXS, Karlsruhe, Germany, 2004.
22. Z. Xia, R. S. Liu, K. W. Huang and V. Drozd, *J. Mater. Chem.*, 2012, **22**, 15183-15189.
23. D. W. Wen, H. Yang, G. H. Yang, J. X. Shi, M. M. Wu and Q. Su, *J. Solid State Chem.*, 2014, **213**, 65-71.
24. J. Y. Sun, Y. N. Sun, J. L. Lai, Z. G. Xia and H. Y. Du, *J. Lumin.*, 2012, **132**, 3048-3052.
25. X. X. Li, Y. H. Wang and Z. Chen, *J. Alloy Compd.*, 2008, **453**, 392-394.
26. J. M. Zheng, C. F. Guo, X. Ding, Z. Y. Ren and J. T. Bai, *Current Applied Physics*, 2012, **12**, 643-647.
27. J. G. Wang, X. P. Jiang, C. H. Yan and J. H. Lin, *J. Electrochem. Soc.*, 2005, **152**, G186-G188.